

8 Dynamics of Vibrationally Mediated Photodissociation of CH₃CFCl₂

The ~235 nm photodissociation of CH₃CFCl₂ pre-excited to three, four and five quanta of C-H methyl stretches was studied to investigate the effect of internal parent excitation on the dynamics of two- and three-body photofragmentation. The ~235 nm photons also tagged spin-orbit ground Cl ²P_{3/2} [Cl] and excited Cl ²P_{1/2} [Cl*] state photofragments, via (2+1) resonance enhanced multiphoton ionization (REMPI) in a time-of-flight (TOF) mass spectrometer. Monitoring the shapes of ³⁵Cl and ³⁵Cl* time-of-arrival profiles revealed their energies and angular distributions showing broad and unstructured fragment kinetic energy distributions. Although a significant amount (~50 %) of the available energy is transferred into internal energy of the CH₃CFCl fragments, the spatial fragment anisotropy is characterized by a non vanishing anisotropy parameter, β , which indicates a fast decay of the parent molecule along the C-Cl dissociation coordinate. Moreover, β for Cl changes from a slightly positive value to a negative value while that of Cl* increases when the pre-excitation is increased from three to five quanta of C-H methyl stretches. This is attributed to the promotion of one of the non-bonding electrons located on the Cl atoms to the σ^* antibonding C-Cl orbital and involvement of several upper states with different symmetry properties.

8.1 Introduction

The hydrochlorofluorocarbons (HCFCs) have reached a fundamental significance since they were introduced as interim replacements for chlorofluorocarbons (CFCs), due to the release of atomic chlorine into the stratosphere and its role in the catalytic ozone destruction cycle. Consequently, photochemistry of the HCFCs is placed in the focus of the attention of atmospheric chemists in order to evaluate the HCFC ozone depletion potential.¹ The interest in HCFC photodissociation is normally linked to fragmentations into two photoproducts. However, at higher dissociation energies, conditions that might be found in the upper stratosphere, three-body decays where molecules split into three photofragments become possible and need to be taken into account for an understanding of atmospheric chemistry.

Apart from their role in atmospheric processes, the dynamics of three-body decays have recently become a subject of research in their own right.^{2,3} Nevertheless, until today, even for photoinduced three-body decays, as the simplest example of elementary three-body chemical processes, only few studies exist leaving an almost unexplored field of chemical reaction dynamics. In particular, studies that test the effect of initial parent nuclear motion on three-body fragmentation are scarce.⁴ Although of high complexity, they can provide new insight into these processes and an understanding of bond breaking. Of particular interest in three-body dissociation is the energy disposal among the emerging fragments and their spatial distribution that might shed light on the involved potential energy surfaces (PESs) and the ensuing dynamics during dissociation.

Vibrationally mediated photodissociation (VMP),^{5,6} in which molecules are prepared in a vibrationally excited state and then promoted by a photon to a dissociative excited state, is now recognized as a method that provides direct means for studying the influence of rovibrational excitation on dynamics. The VMP approach was applied to the two-body fragmentation of several molecular systems including hydrocarbon compounds.^{4,7-15} These studies revealed the effect of the initial state preparation on relative yields of product channels, on internal state distributions and on vector correlations. In particular, in some cases alteration of product identity or distribution in VMP could be found in comparison to the almost isoenergetic one-photon photodissociation.^{7,8,11-14} This is due to sampling of different portions of the upper PES by the vibrationally excited wavefunction and to the participation of more than one PES leading to different adiabatic and nonadiabatic interplay in VMP compared to the one-photon photodissociation.

Like the impact of vibrational pre-excitation on two-body photodissociation processes it is expected that three-body break-up of molecules might also be affected by internal nuclear motion of the parent. The feasibility of corresponding experiments has recently been demonstrated by the evidence for the onset of a three-body decay in the photodissociation of vibrationally excited CHFC_2 .⁴

Halogenated alkane compounds containing two identical halogen atoms are ideal candidates for studying three-body decay. Their electronic configuration lets one expect a localized electron excitation from non-bonding electrons located on the halogen (X) atoms into the anti-bonding σ^* (C-X) orbital,¹⁶ thus weakening both C-X bonds simultaneously

and leading to a direct decay. Three-body decay has been studied in detail for CF₂Br₂¹⁷ and CF₂I₂,¹⁸ which exhibit easily accessible absorption bands above 200 nm and a relatively low three-body decay threshold. For CF₂Br₂ a sequential three-body decay was observed in the wavelength range from 260 to 223 nm whereas for CF₂I₂ a smooth transition took place from a two-body decay to a concerted three-body decay in competition with two different molecular channels upon increasing the energy of the dissociating photon from 3.53 eV (351 nm) to 6.42 eV (193 nm).

VMP studies are greatly facilitated by the existence of chemical bonds where a significant amount of energy can be deposited upon vibrational excitation. To this end, one or more C-H, O-H or N-H bonds are employed to tune the pre-excitation energy over a wide range. In our study of the VMP of CHFCl₂⁴ the evidence for an onset of a three-body decay was observed upon surpassing the three-body decay threshold by increasing the energy of the vibrational pre-excitation of the C-H bond. The VMP of CHFCl₂ pre-excited to the 3₁ and 4₁ C-H polyad components occurs via two-body decay while that of CHFCl₂ (5₁) occurs via both two- and three-body decay. The three-body decay mechanism cannot unequivocally be determined due to the little available energy with respect to the decay into three fragments. Nevertheless, the observed anisotropy parameter, β , of 0.47 for ground state Cl ²P_{3/2} [Cl] atoms suggests a concerted decay in agreement with the expectations from considering the involved molecular orbitals (MOs). Yet, observation of different β values accompanied by different kinetic energy distributions (KEDs) for the spin-orbit states of the chlorine atoms are an evidence of a more complex fragmentation scheme involving excited states of A' and A'' symmetries that probably mix via curve crossing.

Like CHFCl₂, we have recently studied the ~235 nm photodissociation of jet-cooled CH₃CFCl₂ excited with two and three quanta of C-H methyl stretches.¹⁴ The action spectra and the Doppler profiles of the corresponding photofragments were measured, revealing that both Cl and Cl ²P_{1/2} [Cl*] are released as a result of C-Cl bond cleavage. The action spectra were characterised by a multiple peak structure, attributed, relying on a simplified local mode model,^{19,20} to coupling of C-H methyl stretches and deformations. From the area ratios of the Doppler profiles, the Cl*/Cl branching ratio was found to be ~0.5.

In the present work, in continuation of our work on CHFCl₂^{4,15} and the direct photodissociation of CH₃CFCl₂²¹ at 193 nm, we report the results of ~235 nm photodissociation of CH₃CFCl₂^{13,14} excited with three, four, and five quanta of C-H methyl stretches.^{14,20} The molecule was chosen to study the involvement of the different PESs, to examine the role of the three-body channel in VMP and to get insight in the structural dependence of the occurring decay mechanism. The speed distribution $f(v)$ and anisotropy parameters, β , were obtained from the time-of-arrival profiles of ³⁵Cl and ³⁵Cl*. The energy distributions of both Cl and Cl* for molecules prepared in the $\nu_{\text{C-H}} = 3-5$ C-H methyl stretches of CH₃CFCl₂ are broad and similar, ranging from nearly zero center of mass (c.m.) translational energy to the maximal available energy. Therefore, it seems that the energy remains mainly in the parent fragment CH₃CFCl where the internal energy increases with pre-excitation from three quanta of C-H methyl stretches to five. Nevertheless, the energy distribution obtained via five quanta of C-H methyl stretches differs from the three quanta or four quanta states by a tail in the lower energy region in the case of Cl. The small fraction of "slow" photofragments indicates an onset of a three-body channel for the photodissociation via five quanta of methyl stretches where the three-body decay threshold is surpassed. For spin excited Cl* no hint for a three-body decay was observed.

8.2 Experiment

The experiments were carried out in a home-built Wiley-McLaren TOFMS²² similar to that reported previously and shown in Fig. 7.1.¹³⁻¹⁵ The CH₃CFCl₂ sample (98 % purity) prepared as a ~10 % mixture in Ar at a total pressure of 10³ mbar, was expanded through a nozzle-skimmer arrangement. The pressure in the ionization chamber was typically ~8·10⁻⁶ mbar under working conditions. The beam is characterized by a rotational temperature of ~8 K and a vibrational temperature of < 100 K, as estimated from the VMP of propyne-d₃ (3ν₁).¹¹ These temperatures minimize the rotational inhomogeneous structure and the overlap with hot bands in the region of the monitored vibrational states.¹⁴ The source of vibrational overtone excitation (IR/visible) pulses, (typically 6 mJ around 1166.3 nm for preparation of $\nu_{\text{C-H}} = 3$, 10 mJ around 887.4 nm for $\nu_{\text{C-H}} = 4$, and 12 mJ near 727 nm for $\nu_{\text{C-H}} = 5$) was the idler beam of an optical parametric oscillator (bandwidth ~0.08 cm⁻¹). Following the excitation pulse, after a delay of typically 15 ns, the excited

CH₃CFCl₂ molecules were photodissociated by a counterpropagating UV beam (about 120 μJ) from a frequency doubled tunable dye laser (~0.4 cm⁻¹). The wavelength of this beam was chosen to fit the two-photon transition of Cl ($4p^2D_{3/2} \leftarrow 3p^2P_{3/2}$) at 235.336 nm and Cl* ($4p^2P_{1/2} \leftarrow 3p^2P_{1/2}$) at 235.205 nm to tag the photofragments by (2+1) REMPI.²³ The IR/visible beam was focused with a 15 cm focal length (f.l.) lens and the photolysis/probe (UV) beam with a 30 cm f.l. lens. The UV laser photolysed the CH₃CFCl₂ molecules efficiently only when overtone excitation was induced, due to the very low absorption cross section of vibrationless ground state molecules at 235 nm, as shown in Fig. 8.1.²⁴

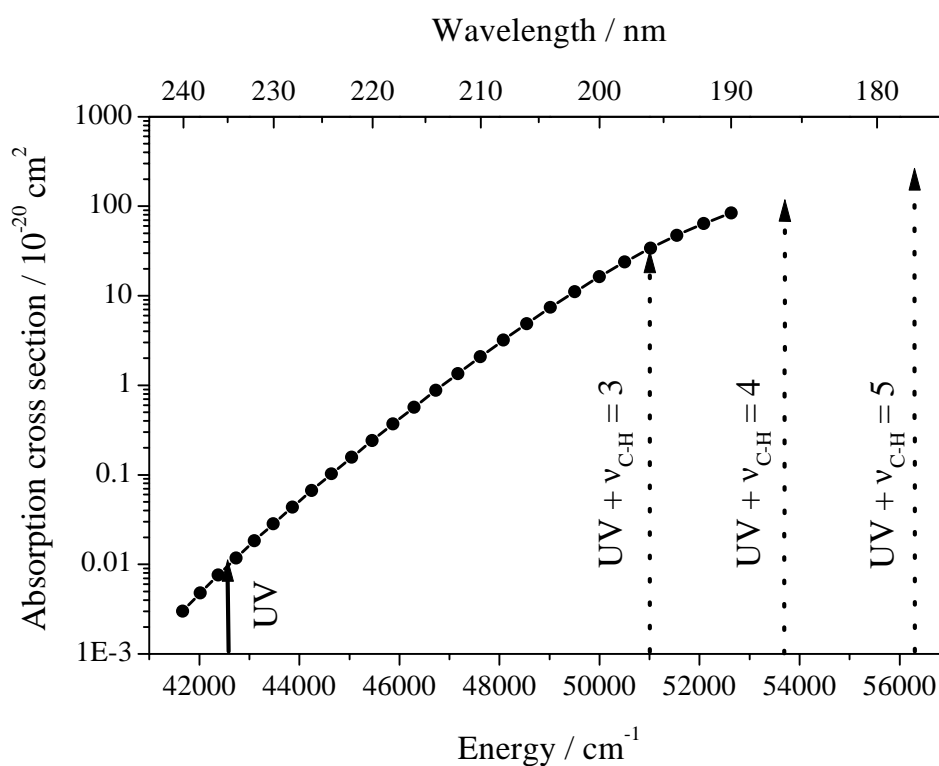


Figure 8.1: Logarithmic absorption cross section of CH₃CFCl₂ based on the publication of Fahr et al.²⁴ The combined wavelength (IR + UV) used in the present experiment are marked by dotted arrows, whereas the ground state photo-dissociation wavelength is marked by a solid arrow. The displayed range is related to the first absorption band of HCFCs (designed as the A band) in the 180-240 nm. This band is broad and unstructured. At high energy the cross section is high decreasing by several orders of magnitude at the red wing. The electronic transition can be described as a $\sigma^* \leftarrow n_{\text{Cl}}$ excitation, involving the promotion of an electron from a nonbonding Cl 2p orbital to an antibonding C-Cl orbital.

Ions formed via REMPI in the focal volume were subjected to continuously biased extraction (-450 V), two acceleration stages (-850 V and -1700 V), two pairs of orthogonal deflection plates and an einzel lens prior to entering the field-free drift region and eventual detection by a microsphere plate. The time-of-arrival profiles of the ^{35}Cl and $^{35}\text{Cl}^*$ resulting from 5000 shots were recorded with a digital oscilloscope and stored on a disk for later analysis. The TOF profiles were taken under space focusing conditions²² at two different geometries, vertical (UV laser polarization perpendicular to the TOF axis) and horizontal (UV laser polarization parallel to the TOF axis). The effect of the apparatus on the time-of-arrival profiles was previously determined⁴ using the approach of Varley and Dagdigian,²⁵ i.e. measurement of the time-of-arrival profiles of ^{35}Cl photofragments from 355 nm photolysis of Cl_2 . These profiles allowed to calibrate the electric field strength, E , in the ionization region, which was found to be 124 V/cm, 12 % lower than the nominal field strength. In addition, the profiles enabled to estimate the apparatus response time and the effective probe laser linewidth that affects the time-of-arrival profiles through Doppler velocity selection along the probe laser direction.²⁵

The KEDs and the anisotropy parameter were extracted from the TOF profiles employing a previously described forward convolution method.⁴

8.3 Results and Discussion

8.3.1 Time-of-Arrival Profiles and their Analysis

Experimental ^{35}Cl and $^{35}\text{Cl}^*$ ion arrival profiles, following the ~235 nm photodissociation of CH_3CFCl_2 prepared in the main peak of the observed multiple peak structure of $\nu_{\text{C-H}} = 3$ -5 vibrational states^{14,20} are displayed in Fig. 8.2 (a) - (c), respectively.

In the case of four quanta of C-H methyl stretches the pre-excitation of the two main peaks observed in the action spectra²⁰ were examined, whereas for $\nu_{\text{C-H}} = 3$ and 5 only the main peak was examined. No significant differences were found for the two different pre-excitation wavelengths in the case of $\nu_{\text{C-H}} = 4$, therefore the results from only the main peak are presented. Although essentially similar distributions were observed, at slightly longer flight times, for the ^{37}Cl fragments, only the portions showing the ^{35}Cl fragments are exhibited. Since the intensity of the signal of ^{35}Cl is three times larger than that of ^{37}Cl , due to its larger natural abundance, analysis of the former was preferred. These profiles

represent the VMP "net" profiles, and were obtained by removing the small contribution, when present, resulting from the ~ 235 nm photodissociation of vibrationless ground state molecules (vibrational excitation laser off) from the signal monitored when both the vibrational excitation laser and the UV laser were on. The contribution from ~ 235 nm photodissociation of vibrationless ground state molecules is low, due to the smallness of the absorption cross section²⁴ of CH_3CFCl_2 at this wavelength.

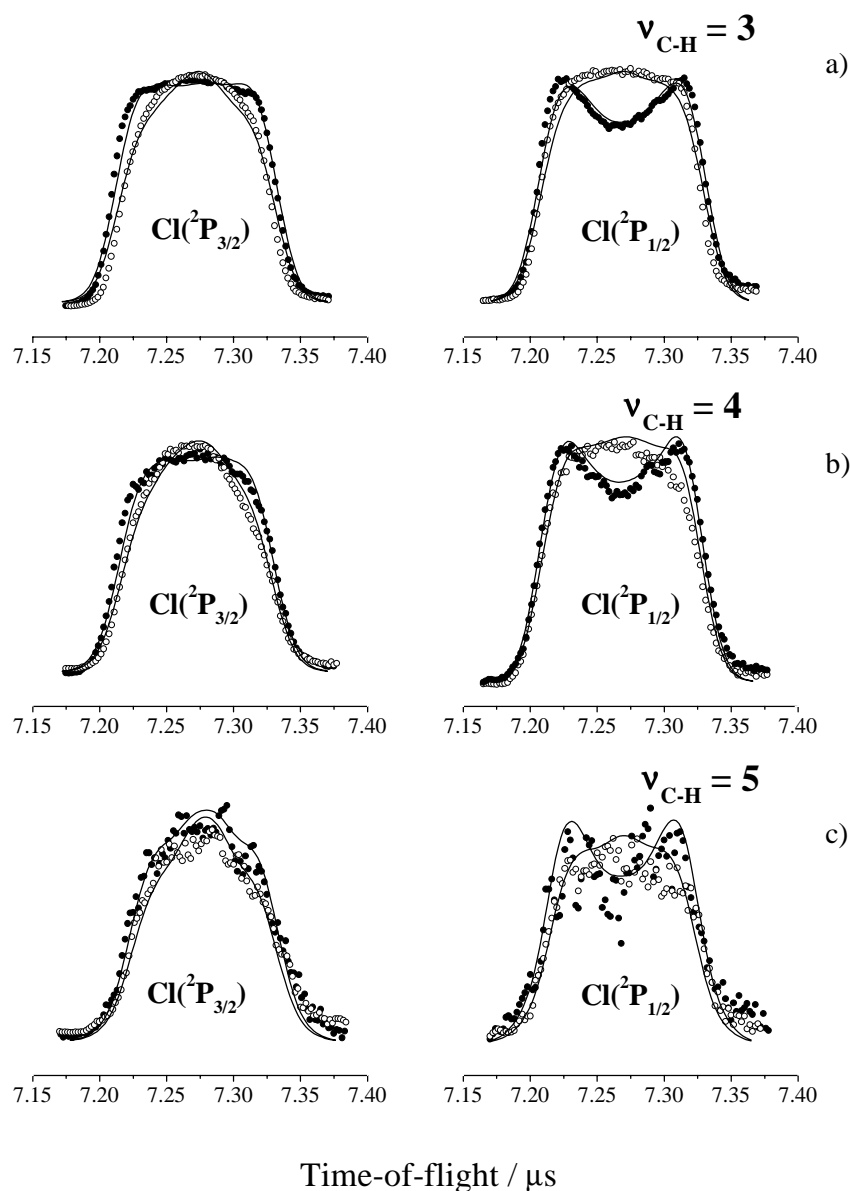


Figure 8.1: Arrival time distributions of $\text{Cl} (^2\text{P}_{3/2})$ and $\text{Cl}^* (^2\text{P}_{1/2})$ photofragments produced in the ~ 235 nm photolysis of CH_3CFCl_2 pre-excited with three quanta (panel a), four quanta (panel b) and five quanta (panel c) of C-H methyl stretches. Solid points and open circles are the experimental data points taken

with the polarization of the UV photolysis/probe laser parallel and perpendicular, respectively, to the TOF MS axis. The polarization of the overtone excitation laser was perpendicular to the TOF MS axis. Solid lines are the simulations of the corresponding profiles. These lines denote the best fit velocity distributions, with constant β , finite time response of the apparatus (modeled as a Gaussian with 20 ns full-width-half-maximum) and Doppler selection by the finite bandwidth of the probe laser (modeled as 0.3 cm^{-1} at the 1-photon wavenumber).

The observed profiles were obtained with the polarization of the photolysis/probe UV laser parallel or perpendicular to the TOF MS axis and with the polarization of the IR/visible vibrational excitation laser axis remaining fixed with perpendicular polarization. The profiles of both Cl and Cl*, taken under these polarization conditions, are shown in Fig. 8.2 (a) – (c).

The main feature in the profiles of Fig. 8.2 is found in the difference between the shapes of the Cl and Cl* spin-orbit components. The ground state Cl photofragment spectra are singly peaked for the parallel and perpendicular polarization of the UV laser, although different widths and profile shapes are noticeable for different UV polarization. The excited state Cl* photofragment spectra are doubly peaked for the parallel and singly peaked for the perpendicular polarization of the UV laser. The profiles obtained for the pre-excitation via five quanta of C-H methyl stretches are noisier due to the smaller transition probability in the vibrational excitation step, but the qualitative behavior remains the same. A doubly peaked TOF profile is observed only if the dissociation process generates a spatially anisotropic fragment distribution with a relatively narrow speed distribution $f(v)$ centered around a large speed value v . The double peaks are due to the formation of photofragments of equal translational energies but with velocity vectors pointing towards and opposite the flight axis. In principle, ion-flyout where particles miss the detector because of small velocity components v_z towards the detector and large velocity components perpendicular to the detector axis would also reduce the middle of the profile, but the acceleration voltages were adjusted so that this effect can be ruled out.

The spatial fragment distribution $P(v, \theta) \propto f(v)(1 + \beta(v)P_2(\cos\theta))^{26,27}$ is characterized by the velocity dependent anisotropy parameter β ranging from -1 (perpendicular transition) to $+2$ (parallel transition), where θ is the angle of the polarization vector of the dissociating

laser with the product recoil velocity vector, and P_2 is the second Legendre polynomial: $P_2(x) = \frac{1}{2}(3x^2 - 1)$. The observed difference in the profile shapes of the different spin-orbit states could in principle be accounted for by a similar speed distribution accompanied by a significantly different anisotropy parameter. However, the calculated β parameter does not vary significantly for Cl and Cl* in the $v_{\text{C-H}} = 3$ and 4 pre-excitation.

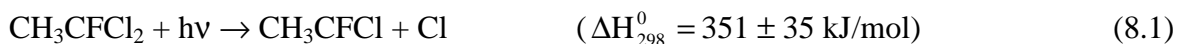
Therefore, the increase in the intensity of the center of the arrival time distribution obtained in VMP of CH₃CFCl₂ $v_{\text{C-H}} = 3-5$ can be attributed to an increase in production of ground state Cl photofragments with nearly zero center of mass (c.m.) translational energies. The difference in the profile shapes for perpendicular and parallel polarization geometries in the case of pre-excitation of $v_{\text{C-H}} = 3$ and 4 indicates that both Cl and Cl* photofragments are released predominantly through a parallel electronic transition with a positive β .^{26,28,29}

To quantitatively extract the β parameters and the c.m. Cl and Cl* photofragment speed distribution, simulations of the TOF profiles were carried out and optimized by a genetic algorithm procedure which minimized the deviation of the simulated profile from the experimentally observed profile. Identical β parameters were used for simultaneously fitting the profiles for both polarization geometries. The simulation procedure has successfully been employed for the dissociation of CHFCl₂.⁴ The best results for the KED obtained by the simulations are shown in Fig. 8.3. As can be seen in Fig. 8.2, the fits to the experimental data are of good quality, although only a single velocity-independent β parameter was employed in the simulation procedure.

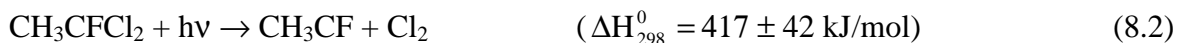
8.3.2 Energy Distributions

The kinetic energy distributions, $P(E)$, and the β parameters obtained for Cl and Cl* photofragments resulting from VMP via three, four, and five quanta of C-H methyl stretches are shown in Fig. 8.3 (a) – (c).

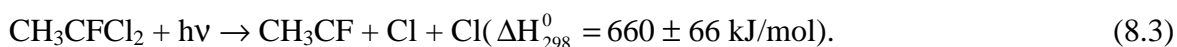
The combined energies (IR/visible + UV) employed in the VMP of CH₃CFCl₂ $v_{\text{C-H}} = 5$ [$\sim 56240 \text{ cm}^{-1}$ (673 kJ/mol)], $v_{\text{C-H}} = 4$ [$\sim 53760 \text{ cm}^{-1}$ (643 kJ/mol)] and $v_{\text{C-H}} = 3$ [$\sim 51070 \text{ cm}^{-1}$ (611 kJ/mol)] exceed that required for the loss of one chlorine atom,



and for the loss of molecular chlorine



but the pre-excitation via $\nu_{\text{C-H}} = 3$ and $\nu_{\text{C-H}} = 4$ does not surpass the threshold for the three-body process where two chlorine atoms are released



The enthalpies, ΔH^0 , of reactions (8.1), (8.2), and (8.3) were calculated for the spin-orbit states with the lowest energy from the standard enthalpies of formation (ΔH_f^0) of the molecule and radicals involved in the process³⁰⁻³² and the errors were calculated as the sum of individual squared errors. The standard enthalpies were partly estimated as arithmetic means from the fully chlorinated and fluorinated species, when data was not available in the literature. The ΔH_{298}^0 required for loss of one or two Cl* atoms are higher than the values given for Cl in reaction (8.1) and (8.3) by 10.6 kJ/mol and 21.2 kJ/mol, respectively.

Taking into account the combined energies channeled into CH₃CFCl₂ molecules and assuming that ΔH^0 equals the C-Cl bond dissociation energy D_0 , the available energy E_{av} and the maximum energetically allowed energies for Cl photofragments were calculated and are shown in Table 8.1. The maximal kinetic energies for Cl and Cl* arising from decay channel (8.1) are indicated by the arrows in Fig. 8.3. In fact the arrows should be shifted to somewhat larger energies if (ΔH_f^0) are retrieved. The energy distributions are centered at relatively high values with tails that reach the maximum Cl energy as Fig. 8.3 clearly shows. The correspondence of the distribution centers to large energies might indicate that the dissociation process occurs on a repulsive PES, as expected from the broad and unstructured first absorption band of CH₃CFCl₂.²⁴

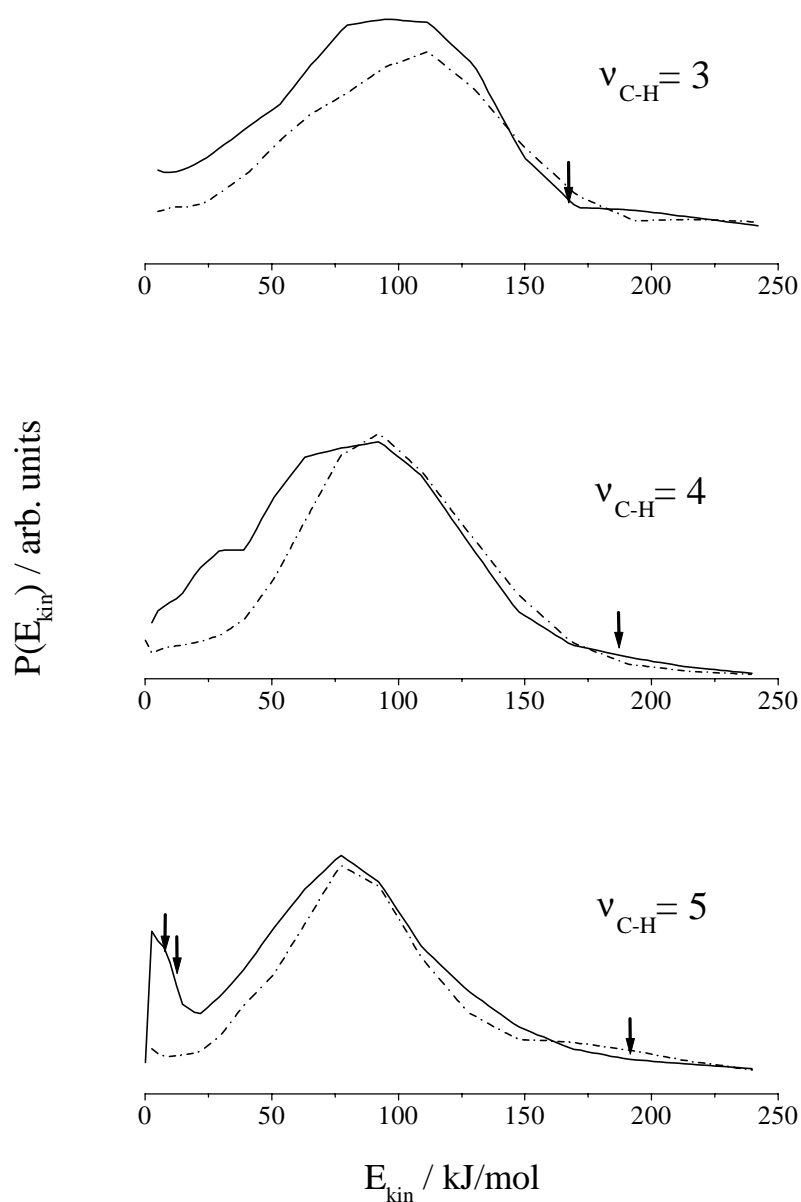


Figure 8.3: Energy distributions of Cl ($^2P_{3/2}$) (solid line) and Cl* ($^2P_{1/2}$) (dashed line) in ~ 235 nm photodissociation of vibrationally excited CH_3CFCl_2 $v_{\text{C-H}} = 3-5$. The distribution was obtained from simultaneous fitting of the parallel and perpendicular profiles. The arrows at the high energies, in the different panels, indicate the maximum possible energies calculated for the two-body photodissociation of CHFCl_2 for three, four, and five quanta of C-H methyl stretches, respectively. The other two arrows in the slow energy region of the bottom panel indicate the maximum allowed energy in the sequential and concerted three-body process, respectively.

In addition, the average translational energy E_T release of the $\text{CH}_3\text{CFCl} + \text{Cl}$ fragment pair via reaction (8.1) is calculated. Since the excess energy E_{av} is known, the translational

energy disposal fraction E_T/E_{av} can be calculated and is shown in Table 8.1 for the different quanta of C-H methyl stretches. In order to compare these values with the recently obtained data for the VMP of CHFC1₂⁴, a detailed, second Table (8.2) is presented.

Table 8.1: Calculated maximal kinetic energies E_{max} , observed mean total \bar{E}_T , fraction of the kinetic energy and the β anisotropy parameters in the photodissociation of vibrationally excited CH₃CFC1₂.

CH ₃ CFC1		E_{preex} (kJ/mol)	E_{max} (kJ/mol)	\bar{E}_T (kJ/mol)	E_{int} (kJ/mol)	E_T/E_{av}	β Parameter
2							
$\nu_{C-H} = 3$	Cl	103	260	119	141	0.46	0.20 ± 0.04
	Cl*		249	131	118	0.53	0.25 ± 0.04
$\nu_{C-H} = 4$	Cl	135	292	112	180	0.38	0.20 ± 0.03
	Cl*		281	126	155	0.45	0.25 ± 0.05
$\nu_{C-H} = 5$	Cl	165	322	106	216	0.33	-0.14 ± 0.05
	Cl*		311	123	188	0.40	0.35 ± 0.06

Table 8.2: Calculated maximal kinetic energies E_{max} , observed mean total \bar{E}_T , fraction of the kinetic energy and the β anisotropy parameters in the photodissociation of vibrationally excited CHFC1₂.

¹ The > symbol is due to the unknown E_T of CHF.

CHFC1 ₂		E_{preex} (kJ/mol)	E_{max} (kJ/mol)	\bar{E}_T (kJ/mol)	E_{int} (kJ/mol)	E_T/E_{av}	β Parameter
3 ₁	Cl	104	276	126	150	0.46	0.14 ± 0.05
	Cl*		265	134	131	0.50	0.36 ± 0.06
4 ₁	Cl	136	308	139	169	0.45	0.27 ± 0.06
	Cl*		297	140	157	0.47	0.43 ± 0.05
5 ₁	Cl	167	339	131	208	0.39	0.47 ± 0.07
Three-body decay			33	> 28 ¹	< 5	0.85	
	Cl*		328	121	207	0.39	0.34 ± 0.04

From estimating the energy release via the impulsive model³³ a value between 0.4 and 0.5 is obtained and therefore the measured values seem to be reasonable. Comparison of these values to those obtained for VMP of CHFCl₂⁴ (3₁) and (4₁) recently in our group (0.45) and by photofragment translational spectroscopy (PTS) experiments by Huber and co-workers³⁴ in 193 nm photodissociation (0.44) shows that the values are in good agreement. Our values are also quite close to those measured for the 193 nm photolysis of other chloromethanes releasing Cl photofragments, including: CHCl₃ [0.43 (Ref. 34) and 0.41 (Ref. 35)], CF₂Cl₂ [0.50 (Ref. 35) and 0.47 (Ref. 36)], CFCl₃ [0.43 (Ref. 35) and 0.47 (Ref. 37)] and CCl₄ [0.35 (Ref. 35)]. This implies that a rather high kinetic energy release occurs in the photodissociation of vibrationally excited CH₃CFCl₂ similarly to the photodissociation of other vibrationless ground state molecules and of vibrationally excited CHFCl₂, agreeing with a direct dissociation process on a repulsive surface. As stated by Huber³⁴ and by Gentry³⁵ and their co-workers, their translational energy disposal fraction, and also ours for CHFCl₂ and CH₃CFCl₂, differ from those obtained by Matsumi et al.³⁸ They probed the Cl atoms by REMPI and measured the Doppler profiles in 193 nm photodissociation of several chloromethanes. The E_T/E_{av} that they obtained were much higher, i.e. 0.85 for CHCl₃ and 0.78 for CH₃Cl. With respect to the latter values it must be taken into account that an integrative method like Doppler profile analysis generally tends to underestimate the contribution of slow particles, especially if the speed distribution is broad.

It is noteworthy that the calculated values of the \overline{E}_T shown in Table 8.1 remain constant, within experimental error, upon pre-excitation with three to five quanta of C-H methyl stretch. Observing a constant \overline{E}_T while increasing the combined energy, one might expect a barrier in the exit channel of the upper PES where the constant barrier height determines the kinetic energy release. But this scenario is highly unlikely from MO considerations, from the observed anisotropy and from the unstructured absorption spectrum all of which hint at a direct, barrierless dissociation on a repulsive surface. Moreover, structurally similar molecules were found to dissociate directly and fast in the dissociation coordinate.^{17,34} However, in CH₃CFCl₂ there is no significant additional energy flow into the dissociation coordinate upon increasing C-H methyl stretches excitation as observed in the case of CHFCl₂, where \overline{E}_T increased from 126 kJ/mol to 139 kJ/mol upon pre-excitation via three to four quanta of C-H methyl stretches. This observation can be explained by the following arguments: as the time period between the pre-excitation and

the dissociation is by far long enough for a complete redistribution¹⁴ which occurs on a sub-nanosecond timescale, the pre-excitation energy via three, four, and five quanta of C-H methyl stretches will be distributed over the 18 normal modes in the CH₃CFCl₂ molecule.³⁹ Total equipartitioning of the pre-excitation energy on all vibrational degrees of freedom leads to an additional energy flow of 950, 1250, and 1530 cm⁻¹, respectively, into the C-Cl dissociation coordinate. Therefore, only one or two quanta of C-Cl stretch will be populated taking a typical vibrational quantum of 600 cm⁻¹ into account.⁴⁰ The corresponding increase of the kinetic energy of the ejected Cl atoms is so small that it is not observable due to the experimental resolution. Whereas in the case of CHFCl₂, a smaller molecule with only 9 normal modes, the increase of the kinetic energy of the Cl atoms from photodissociation of 3₁ to 4₁ is noticeable, while via 5₁ the three-body decay channel starts to contribute by adding low kinetic energy fragments. This observation hints at a similar shift for the ground and excited state surface in the reaction coordinate by approximately the value of the internal energy of the partner fragment CH₃CFCl or CHFCl whereas the small additional kinetic energy is induced by only few quanta of C-Cl stretches.⁴¹

The very slow Cl photofragments, observed in the VMP of CH₃CFCl₂ via five quanta of C-H methyl stretches, might emerge from the synchronous concerted three-body decay, where two C-Cl bonds are broken simultaneously, or from a sequential three-body decay.^{2,3} For the former the maximum allowed Cl velocity is 610 m/s (6.5 kJ/mol) and for the latter 720 m/s (9.1 kJ/mol), as indicated by the corresponding arrows of the bottom panel of Fig. 8.3. It is noteworthy that the calculated maximum energies, based on the above enthalpies for reaction, suffer from inaccuracies due to the relatively large uncertainties in the enthalpies. The slow atoms contribute to less than 4 % to the total Cl fragments, whereas in the case of CHFCl₂ the contribution of the three-body decay channel was about 10 %. Thus the dynamics of the three-body decay cannot be verified. In the case of Cl* no slow atoms were observed which is not surprising due to the very small available energy which would lead to maximal speeds of 270 m/s.

8.3.3 Anisotropies

The electronic configuration of the ground state is:

$$\dots (17a')^2(10a'')^2(11a'')^2(18a')^2(12a'')^0(19a')^0$$

Both unoccupied $(12a'')^0$ and $(19a')^0$ MOs are C-Cl anti-bonding. The occupied $(17a')^2$, $(10a'')^2$, $(11a'')^2$, and $(18a')^2$ are non-bonding MOs composed of the 3p-electrons of the Cl atoms. Single electron excitation gives rise to eight states of A' and A'' symmetry which are the result of electron excitation from non-bonding electrons located at the Cl atom into anti-bonding C-Cl MOs ($\sigma^*(\text{C-Cl}) \leftarrow n(\text{Cl})$) leading to a direct decay.

The magnitude and sign of β are related to the symmetry of the ground and excited state, the orientation of the transition dipole moment μ in the parent molecule and the excited state lifetime. The theoretical limit for the β parameter, with μ parallel to the line connecting the two Cl atoms, is estimated to be ~ 1.1 for the transition $A'' \leftarrow A'$ (based on a Cl-C-Cl bond angle of 112° in CH₃CFCl₂) and in the range from -1 to 0 for the transition $A' \leftarrow A'$ as the CH₃CFCl₂ molecule belongs to the C_s symmetry group.

The recoil anisotropies provide essential information regarding the mechanism of bond breaking. The β parameters extracted from the experimental data are shown in Table 8.1. Errors were calculated from the scattering of the 10 "best" β parameters obtained by the data analysis procedure described above. Relying on the data in Table 8.1, it is seen that the Cl and Cl* arising from ~ 235 nm photodissociation of CH₃CFCl₂ $\nu_{\text{C-H}} = 3$ and $\nu_{\text{C-H}} = 4$ via two-body processes (8.1) possess positive anisotropies with almost constant values, lower than the limiting values.

The β values obtained in the VMP experiment via $\nu_{\text{C-H}} = 3$ and $\nu_{\text{C-H}} = 4$ are positive, thus ruling out a pure $A' \leftarrow A'$ excitation, but lower than the limiting values for the pure $A'' \leftarrow A'$ transition. Relying on the direct excitation of C-Cl antibonding MOs the dissociation should be prompt and it does not seem likely that the rotational motion accounts for the reduction of β from its limiting value. If only rotation of the parent molecule⁴² is responsible for the reduction of β , then a lifetime of $\tau = 172$, 57 , and 32 fs is

estimated based on the temperature 10, 100, and 300 K, respectively and an equilibrium bond angle of 86°. These small limiting lifetimes are a consequence of the large moments of inertia for the CH₃CFCl₂ leading to fast loss of anisotropy due to molecule rotation. Thus, for a bulk experiment at 300 K it should be virtually impossible to observe the limiting β parameter values even for a direct decay. Under molecular beam conditions ($T_{\text{rot}} = 10$ K, $T_{\text{vib}} = 100$ K) however, a significantly higher β parameter than the observed values of 0.2 to 0.3 would be expected for a direct fragmentation process. Consequently the observation of less than limiting β values should emerge from dynamical factors or from the simultaneous excitation of A' and A'' states, that probably mix via curve crossing to release both photofragments. From the measured β and the spin-orbit state branching ratio¹⁴, it is inferred that both Cl and Cl* in $\nu_{\text{C-H}} = 3$ and $\nu_{\text{C-H}} = 4$ photodissociation are produced as a result of simultaneous absorption to A'' and A' states.

Due to the decrease of β corresponding to Cl via $\nu_{\text{C-H}} = 5$, it is likely that the contribution of an excited state of A' symmetry increases. If the involved A' state responsible for the observed β value were identical to the A' state which was found to release predominantly Cl* atom, an increase in the Cl*/Cl branching ratio would be expected. However, a decrease was found in this ratio from 0.36 to 0.16 upon increasing the dissociation energy from 235 nm to 193nm,^{14,21} whereas the ratio is about 0.5 via 235 nm photodissociation pre-excited with three and four quanta of methyl stretches. Therefore it seems that at least three different upper states are involved in the CH₃CFCl₂ photolysis in the 40000 – 56000 cm⁻¹ energy range.

The contribution of the three-body decay is small (< 4 %) although after population of the anti-bonding σ^* (C-Cl) orbital for both Cl one would expect a dominant three-body decay while passing the energy limit for it. The insignificant contribution is probably due to the small available energy for the three-body decay. For CHFCl₂ evidence of the onset of three-body decay was observed upon surpassing the energetic threshold as a consequence of the larger vibrational excitation of the dissociation coordinate.

In view of the above discussed MOs a participation of the molecular channel ($\text{CH}_3\text{CFCl}_2 + h\nu \rightarrow \text{CH}_3\text{CF} + \text{Cl}_2$) is unlikely. Although the 19a' MO is anti-bonding in both C-Cl bonds, the Cl (3p) atomic orbitals contributing to the 19a' MO of CH₃CFCl₂ do not correlate to the ground state Cl₂ σ -bond for the formation of a stable Cl₂ molecule.

All in all the pre-excitation seems to be insignificant for the energetics, but very important for the involvement of the upper states leading to a different spin-orbit branching ratio relative to 193 nm photodissociation of vibrationless ground state CH₃CFCl₂¹⁴ and an enormous increase in the signal intensity due to the improved Frank-Condon-factors and the different upper PES which are accessed.

8.4 Conclusions

The VMP of CH₃CFCl₂ pre-excited with three, four, and five quanta of C-H methyl stretches was studied using the REMPI-TOF technique for the measurement of time-of-arrival profiles of Cl and Cl* photofragments. The data analysis yielded the photofragment energy distributions and the recoil anisotropy parameters. These results suggest that the photodissociation of CH₃CFCl₂ $\nu_{\text{C-H}} = 3, 4, \text{ and } 5$ occurs via two-body decay. The upper limit for the contribution of the three-body decay via CH₃CFCl₂ $\nu_{\text{C-H}} = 5$ is 4 % of the total. The \overline{E}_T distributions change only insignificantly upon increasing the excitation energy from three to five quanta hinting at a fast dissociation and a similar shift of both the ground and excited state energies with respect to the dissociation coordinate. Most of the excitation energy remains in the partner fragment CH₃CFCl with increasing internal energy.

While the effect of the vibrational excitation on the kinetic energy distribution of the fragment is small, spatial fragment distribution, branching ratios and the signal intensity are significantly affected by the amount of initially deposited vibrational energy. The anisotropy parameters range from -0.2 to 0.3. They are lower than the limiting value of 1.1 for a pure A'' ← A' excitation indicating that both A' and A'' states are involved, which mix via curve crossing to release Cl and Cl*. No significantly different behavior was found for Cl and Cl* except for Cl resulting from the photodissociation of CH₃CFCl₂ excited to five quanta of C-H methyl stretch. Most likely the large combined excitation energy allows accessing an additional A' state, which predominantly correlates to Cl, thus lowering the effective β parameter. In comparison to the measurement of the photodissociation of vibrationally excited CHFCl₂ we conclude that the additional methyl group influences the mechanism of the decay. Purely energetic effects due to the increased total (combined) energy become negligible whereas the modified vibrational wavefunction of the electronic

ground state results in accessing different parts of the upper PES in a basically constant energy range.

8.5 Acknowledgement

We are grateful to Dr. A. Melchior and Dr. A. Chichinin for numerous stimulating discussions. This research was supported by the German-Israeli Foundation (GIF) under Grant No. I 0537-098.05/97 and by the James Franck Binational German-Israeli Program in Laser-Matter Interaction. T. E. gratefully acknowledges the financial support by the Fonds der Chemischen Industrie and the Minerva Foundation.

-
- ¹ Wayne, R. P. *The Chemistry of Atmospheres*, 2nd ed. (Oxford University Press: Oxford, 1991).
 - ² C. Maul and K.-H. Gericke, *Int. Rev. Phys. Chem.* **16**, 1 (1997).
 - ³ C. Maul and K.-H. Gericke, *J. Phys. Chem A* **104**, 2531 (2000).
 - ⁴ X. Chen, R. Marom, S. Rosenwaks, I. Bar, T. Einfeld, C. Maul, and K.-H. Gericke, *J. Chem. Phys.* **114**, 9033 (2001).
 - ⁵ F. F. Crim, *J. Phys. Chem.* **100**, 12725 (1996); and references therein.
 - ⁶ I. Bar and S. Rosenwaks, *Int. Rev. Phys. Chem.* **2**, 711 (2001); and references therein.
 - ⁷ E. Woods III, H. L. Berghout, C. M. Cheatum, and F. F. Crim. *J. Phys. Chem. A* **104**, 10356 (2000); M. J. Coffey, H. L. Berghout, E. Woods III, and F. F. Crim. *J. Chem. Phys.* **110**, 10850 (1999).
 - ⁸ J. Zhang, C. W. Riehn, M. Dulligan, and C. Wittig, *J. Chem. Phys.* **103**, 6815 (1995).
 - ⁹ R. P. Schmid, T. Arusi-Parpar, R.-J. Li, I. Bar, and S. Rosenwaks, *J. Chem. Phys.* **107**, 385 (1997); R. P. Schmid, Y. Ganot, I. Bar, and S. Rosenwaks, *J. Chem. Phys.* **109**, 8959 (1998).
 - ¹⁰ R. P. Schmid, Y. Ganot, I. Bar, and S. Rosenwaks, *J. Molec. Struct.* **197**, 480 (1999); T. Arusi-Parpar, R. P. Schmid, R.-J. Li, I. Bar, and S. Rosenwaks, *Chem. Phys. Lett.* **268**, 163 (1997).
 - ¹¹ X. Chen, Y. Ganot, I. Bar, and S. Rosenwaks, *J. Chem. Phys.* **113**, 5134 (2000).
 - ¹² H. M. Lambert and P. J. Dagdigian, *J. Chem. Phys.* **109**, 7810 (1998); H. M. Lambert and P. J. Dagdigian, *Chem. Phys. Lett.* **275**, 499 (1997); A. Melchior, H. M. Lambert, P. J. Dagdigian, I. Bar, and S. Rosenwaks, *Isr. J. Chem.* **37**, 455 (1997).
 - ¹³ A. Melchior, X. Chen, I. Bar, and S. Rosenwaks, *Chem. Phys. Lett.* **315**, 421 (1999).
 - ¹⁴ A. Melchior, X. Chen, I. Bar, and S. Rosenwaks, *J. Chem. Phys.* **112**, 10787 (2000).
 - ¹⁵ A. Melchior, X. Chen, I. Bar, and S. Rosenwaks, *J. Phys. Chem. A* **104**, 7927 (2000).
 - ¹⁶ M. B. Robin, *Can. J. Chem.* **63**, 2032 (1985).
 - ¹⁷ M. R. Cameron, S. A. Jones, G. F. Metha, and S. H. Kable, *Phys. Chem. Chem. Phys.* **2**, 2539 (2000).

- ¹⁸ E. A. J. Wannemacher, P. Felder, and J. R. Huber, *J. Chem. Phys.* **95**, 986 (1991), G. Baum, P. Felder, and J. R. Huber, *J. Chem. Phys.* **98**, 1999 (1993). K. Bergmann, R. T. Carter, G. E. Hall, and J. R. Huber, *J. Chem. Phys.* **109**, 474 (1998); W. Radloff, P. Farmana, V. Stert, E. Schreiber, and J. R. Huber, *Chem. Phys. Lett.* **291**, 173 (1998); H. A. Scheld, A. Furlan, and J. R. Huber, *Chem. Phys. Lett.* **326**, 366 (2000).
- ¹⁹ J. L. Duncan, C. A. New, and B. Leavitt, *J. Chem. Phys.* **102**, 4012 (1995).
- ²⁰ X. Chen, A. Melchior, I. Bar, and S. Rosenwaks, *J. Chem. Phys.* **112**, 4111 (2000).
- ²¹ A. Melchior, I. Bar, and S. Rosenwaks, *J. Chem. Phys.* **107**, 8476 (1997).
- ²² W. C. Wiley and I. H. McLaren, *Rev. Sci. Instrum.* **26**, 1150 (1955).
- ²³ R. Liyanage, Y. Yang, S. Hashimoto, R. J. Gordon, and R. Field, *J. Chem. Phys.* **103**, 6811 (1995).
- ²⁴ A. Fahr, W. Braun, and M. J. Kurylo, *J. Geophys. Res.* **98**, 20467 (1993).
- ²⁵ D. F. Varley and P. J. Dagdigian, *J. Phys. Chem.* **99**, 9843 (1995).
- ²⁶ R. N. Zare, *Mol. Photochem.* **4**, 1 (1972).
- ²⁷ M. Mons and I. Dimicoli, *J. Chem. Phys.* **90**, 4037 (1989).
- ²⁸ G. E. Hall and P. L. Houston, *Annu. Rev. Phys. Chem.* **40**, 375 (1989).
- ²⁹ R. J. Gordon and G. E. Hall, *Adv. Chem. Phys.* **96**, 1 (1996).
- ³⁰ M. W. Chase, NIST-JANAF, Thermochemical Tables, Fourth Edition, *J. Phys. and Chem. Reference Data*, Monograph 9, Part I + II (1998).
- ³¹ W. B. DeMore, S. P. Sander, D. M. Golden, R. F. Hampson, M. J. Kurylo, C. J. Howard, A. R. Ravishankara, C. E. Kolb, and M. J. Molina, JPL Publication 92-20 (1992).
- ³² S. Y. Chiang, Y. C. Lee, and Y. P. Lee, *J. Phys. Chem. A* **105**, 1226 (2001).
- ³³ H. Okabe, *J. Chem. Phys.* **53**, 3507 (1970); *Photochemistry of Small Molecules* (Wiley-Interscience, New York, 1978).
- ³⁴ X. Yang, P. Felder, and J. R. Huber, *Chem. Phys.* **189**, 127 (1994).
- ³⁵ M. D. Nachbor, C. F. Giese, and W. R. Gentry, *J. Phys. Chem.* **99**, 15400 (1995).
- ³⁶ G. Baum and J. R. Huber, *Chem. Phys. Lett.* **203**, 261 (1993).
- ³⁷ P. Felder and C. Demuth, *Chem. Phys. Lett.* **208**, 21 (1993).
- ³⁸ Y. Matsumi, K. Tonokura, M. Kawasaki, G. Inoue, S. Satyapal, and R. Bersohn, *J. Chem. Phys.* **94**, 2669 (1991); *ibid.*, **97**, 5261 (1992).
- ³⁹ T. J. Minehardt, J. David Adcock, and R. E. Wyatt, *Chem. Phys. Lett.* **303**, 537 (1999), and references therein.
- ⁴⁰ L. J. Bellamy, *The Infrared Spectra of Complex Molecules and Advances in Infrared Group Frequencies* (Chapman and Hall, London 1958 and 1968).
- ⁴¹ R. Schinke, *Photodissociation Dynamics*, Cambridge Monographs on Atoms, Molecular and Chemical Physics 1 (Cambridge University Press, 1993).
- ⁴² G. E. Busch and K. R. Wilson, *J. Chem. Phys.* **56**, 3638 (1972).